XLI CILAMCE
XLI Ibero-Latin American Congress on Computational Methods in Engineering
16-19 November, 2020 FOZ DO IGUAÇU PARANÁ - BRAZIL

Investigation of Soil Effects on the Fatigue Behaviour of an Offshore Wind Turbine

Fellipe A. Gomes[1], Gilberto B. Ellwanger[1], José R. M. de Sousa[1]

[1]*Dept. of Civil Engineering, Federal University of Rio de Janeiro*
Av. Athos da Silveira Ramos, 149, 21941-909, Ilha do Fundão, Rio de Janeiro, Brazil
fellipe.gomes@coc.ufrj.br
gbe@coc.ufrj.br
jrenato@laceo.coppe.ufrj.br

Abstract. Fatigue is a governing limit state for the design of an offshore wind turbine (OWT). The fatigue loads are not only strongly dependent on the action of waves and wind but also on the site-specific soil properties. The present article is aimed at investigating the effects of cohesive and non-cohesive soils on the fatigue damage of a monopile foundation in water depth of 20 meters, using SIMA-RIFLEX for coupled aero-hydro-servo-elastic simulations and TurbSim for spatio-temporal stochastic wind speed generation. The turbine model is based on the 5-MW reference wind turbine described by NREL (National Renewable Energy Laboratory) and the soil-structure interaction is simulated by applying p-y curves proposed by API-RP-2GEO (2011) and DNVGL-ST-0126 (2016). Fatigue damage is estimated with use of rainflow counting (RFC) method, which is used in combination with Palmgreen-Miner rule and S-N curve proposed by DNVGL-RP-C203 (2016). It was identified that, depending on the soil type, the degree of fatigue damage can vary as well as the critical region along the monopile.

Keywords: Offshore wind turbine, Fatigue analysis, Soil-structure interaction, Monopile

1 Introduction

The world has been experiencing an exponential growth in terms of offshore wind installed capacity, reaching a cumulative power capacity greater than 29 GW (Lee and Zhao [1]). Many of this wind power is generated by offshore wind turbines (OWTs) that are supported by monopile, as this type of foundation has proved to be a economical choice when considering shallow water depth. However, due to its high length-diameter (L/D) ratio, ranging from 3 to 8, this type of structures is very susceptible to dynamic loads induced by wind and wave action.

Adding to this, it must withstand the forcing loads generated by the operational frequency of the turbine. This dynamic excitation is produced by the speed in which the rotor operates, the so-called 1P frequency, and also by the blade passing frequency, which is called 3P frequency. Due to this, designers must pay close attention to the natural frequency of the structure, always looking forward to prevent resonance. To do so, it is of utter importance to consider the soil-structure interaction, because it may change the stiffness of the structure and, consequently, the resonance frequency.

In this paper, the fatigue limit state (FLS) of a monopile foundation, in water depth of 20 meters, is analysed in order to identify the effects that cohesive and non-cohesive soils may have on the fatigue damage of an OWT. The soil-structure interation is based on the model proposed by Winkler, which considers the soil resistance as a spring with stiffness given by the p-y method.

2 Reference Turbine Model and Support Structure

2.1 NREL 5MW baseline offshore wind turbine

The model used for the analyses was the same as proposed in Gomes [2], which is based on the NREL 5MW reference wind turbine, however, with the transition piece included. It has a hub height of 90 m relative to the sea water level, a rotor diameter of 126 m and, most importantly for fatigue design, a turbine operation period

ranging from 5 to 8.6 seconds (1P frequency), with a blade passing period varying from 1.65 to 2.86 seconds (3P frequency) (Jonkman et al. [3]).

The structure was modeled in RIFLEX, which is a modeling tool developed by MARINTEK [4]. This software allows the user to consider coupled non-linear aero-hydro-servo-elastic simulations. Blades, tower and monopile were modeled as axisymmetric pipe with Young's modulus E = 210 MPa and shear modulus G = 80.8 MPa. The monopile considered in this work has 6 m in diameter, thickness of 0.06 m, and an embedment length of 36 m.

2.2 Soil-structure interaction

In this study, the lateral system response is obtained using the beam on, the so-called, nonlinear Winkler foundation model. As a consequence, the monopile was discretized into beam elements of 1.0 meter, each one of them attached to a equaly spaced soil spring. The spring force is computed in accordance with the relationship between the soil resistance "p" and the pile deflection "y", which is obtain from the p-y curves proposed by API-RP-2GEO [5] and DNVGL-ST-0126 [6]. As for the vertical system response, the structure was considered to be vertically restrained.

For the analysis in cohesive soil ($s_u < 100kPa$), the ultimate lateral resistance is described as:

$$p_u = \begin{cases} (3s_u + \gamma' z)D + Js_u z, & \text{if } 0 < z \leq z_r \\ 9s_u D, & \text{otherwise} \end{cases} \tag{1}$$

the p-y curve, for cyclic loading and $z > z_r$, is defined as:

$$p = \begin{cases} \frac{p_u}{2}(\frac{y}{y_c})^{1/3}, & \text{if } y \leq 3y_c \\ 0.72p_u, & \text{otherwise} \end{cases} \tag{2}$$

and the p-y curve, for cyclic loading and $z \leq z_r$, is defined as:

$$p = \begin{cases} \frac{p_u}{2}(\frac{y}{y_c})^{1/3}, & \text{if } y \leq 3y_c \\ 0.72p_u(1 - (1 - \frac{z}{z_r})\frac{y - 3y_c}{12y_c}), & \text{if } 3y_c < y \leq 15y_c \\ 0.72p_u\frac{z}{z_r}, & \text{otherwise} \end{cases} \tag{3}$$

where z_r describes the depth below soil surface, in meters, where the ultimate lateral resistance exceeds the limit of $9s_uD$, D is the pile diameter in m, γ' is submerged unit weight in kN/m^3, s_u is the undrained shear resistance in kPa, y_c is the deflection at one half the ultimate soil resistance, estimated as $(2.5\epsilon_c D)$, and, finally, ϵ_c and J are parameters that describe the load-deflection curve.

For the analyses it was chosen 3 different values for the undrained shear resistance 10kPa, 20kPa and 50kPa. The values for ϵ_c were taken in accordance to Table 1 (Ruigrok [7]).

Table 1. s_u and ϵ_c relationship (adapted from Ruigrok [7])

Consistency	ϵ_c [-]	s_u [kPa]
Very soft	0.02	< 13
Soft	0.02	13-25
Firm	0.01	25-50

Others parameters adopted were J=0.5 and submerged unit weight of $8.5kN/m^3$.

As for the non-cohesive soil, 3 different soils with 25°, 30° and 35° were analysed. The ultimate lateral resistance for this type of soil is described as:

$$p_u = \begin{cases} (C_1(\phi)z + C_2(\phi)D)\gamma' z, & \text{for shallow depth} \\ C_3(\phi)D\gamma' z, & \text{for deep depth} \end{cases} \tag{4}$$

and the p-y curve, for cyclic loading, is defined as:

$$p = 0.9p_u tanh\left(\frac{kz}{0.9p_u}y\right) \tag{5}$$

where $C_1(\phi)$, $C_2(\phi)$ and $C_3(\phi)$ are coefficients that depend on the internal angle o friction (ϕ) and k is the initial modulus of subgrade reaction, which can also be obtain by a given internal angle o friction (ϕ), as provided in Table 2 (ISO-19902 [8]).

Table 2. ϕ and k relationship (adapted from ISO-19902 [8])

Descriptive term	Internal angle of friction	MN/m^3
Very loose	25°	5,4
Loose	30°	11
Medium dense	35°	22

Please note, with increasing undrained shear resistance and increasing internal angle of friction, the initial soil spring stiffness is also increased. It can be seen in Fig. 1(a), for cohesive soil and in Fig. 1(b), for non-cohesive soil. This behaviour draws attention to the importance of conducting coupled soil-structure analyses when it comes to OWT, as it may affect the natural frequency and consequently its dynamic response to external loading.

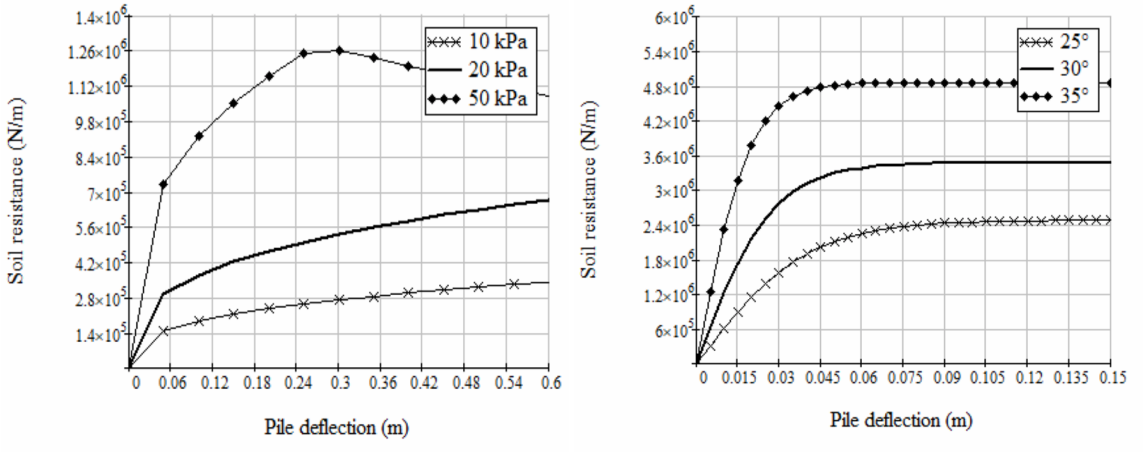

(a) Cohesive p-y curve at 12m depth

(b) Non-cohesive p-y curve at 12m depth

Figure 1. Extracted p-y curves for cohesive and non-cohesive soil.

2.3 Natural period

As discussed, OWTs are prone to dynamic excitation due to turbine operation, wave and wind incidence. Consequently, it is interesting to consider the effect that the soil properties may have on the natural period of the

lowest mode of vibration. In this study, it is possible to see a correlation between the initial soil stiffness of the p-y curve with the natural period of the structures in cohesive and non-cohesive soil, respectively. The greater the inclination of the curve in Fig. 1(a) and in Fig. 1(b), the lower is the natural period in Table 3. This is in agreement with what one must expect to happen, considering that the system has the same mass, but increasing stiffness.

Table 3. First resonance periods according to soil type

Undrained shear strength	Natural period (fore-aft)	Angle of friction	Natural period (fore-aft)
10 kPa	4.63 s	25°	4.06 s
20 kPa	4.52 s	30°	3.97 s
50 kPa	4.25 s	35°	3.89 s

3 Environmental Conditions

The environmental conditions were taken as the same as provided in Gomes [2], for the design load case (DLC) 1.2 (Table 4). It was based on the Campos Basin data provided in Gonçalves et al. [9], with co-diretional, unidiretional wind and wave. Current was not considered as it may introduce an additional damping to the system, possibly reducing the damage (IEC-61400-3 [10]).

Table 4. Environmental condition (adapted from Gomes [2])

Environmental State	V_{hub} [m/s]	H_s [m]	T_p [s]	Frequency Factor [-]
E1	4	3.7	11.4	8.99E-02
E2	6	4.3	11.9	3.24E-02
E3	8	4.8	12.4	1.28E-02
E4	10	5.2	12.7	5.37E-03
E5	12	5.5	13.1	2.35E-03
E6	14	5.9	13.4	1.06E-04
E7	16	6.1	13.7	4.92E-04
E8	18	6.4	14	2.34E-04
E9	20	6.7	14.2	1.13E-04
E10	22	6.9	14.7	5.56E-05
E11	24	7.1	14.9	2.77E-05

In order to consider the wind loads as realistic as possible, it was used TurbSim (Jonkman and Kilcher [11]), a software capable of simulate stochastic and full-field turbulent wind velocity. It was used a Kaimal spectral model with turbulence intensity of 14% and power law exponent of 0.14, which is in accordance with IEC-61400-3 [10] wind class IIB. For the arodynamic loads, RIFLEX applies the blade element momentum (BEM) theory (MARINTEK [4]). As for the hydrodynamic loads, it was used JONSWAP spectrum combined with Morison's equation, applying a drag coefficient of 0.9 and a mass coefficient of 2, as per Velarde and Bachynski [12].

Time domain simulations were conducted with a time step of 0.01 seconds. Simulations of 3800 seconds were applied for each environmental condition, with a cut-off of 200 seconds in order to remove the transient period. Moreover, the structural damping was given by Rayleigh model, with a damping ratio of 2%.

4 Fatigue Damage Calculation

It was taken 5 representative regions along the monopile, based on its diameter D=6 m, at the mudline (z=0m), at 1D (z=-6.5 m), at 2D (z=-12.5 m), at 3D (z=-18.5 m) and at 4D (z=-24.5 m). In all these regions, the stress-time series was calculated considering only the bending moment, as given in eq. (6).

$$\sigma = \frac{M_y}{I_y} r cos(\theta) + \frac{M_z}{I_z} r sin(\theta) \tag{6}$$

where I_y and I_z are the cross-section moment of inertia, M_y and M_z are the moment about the local y and z axis, r and θ is the radial position.

The fatigue damage is computed using the rainflow counting (RFC) algorithm, and Palmgren-Miner's rule for linear fatigue damage accumulation. This procedure is extensively applied in the offshore industry and makes use of S-N curves proposed by DNVGL-RP-C203 [13] in order to estimate the structural damage caused by each stress cycle. For this work, it was used the curve C1 for structures in seawater with cathodic protection.

5 Simulation Results and Discussion

5.1 Critical region for cohesive and non-cohesive soil

The results for selected regions along the monopile in cohesive and non-cohesive soil is shown in Fig. 2, which also shows the contribution of each environmental state for the damage. Depending on the soil type, the maximum fatigue damage experienced by the monopile varied between 1D (-6.5 m) and 4D (-24.5 m).

For the non-cohesive soil the critical region was clear to identify rather than it was for the cohesive. The former had its critical region localized around 1D (-6.5 m), whereas the latter had its critical region ranging from 2D (-12.5 m) to 4D (-24.5 m). This pattern can also be seen in the maximum bending moment envelop extracted from analyses, shown in Fig. 3. It is clear to see that the maximum moment is localized in different regions for each soil type, but with great similarities to the critical regions pointed out by the fatigue damage simulation. This behavior can be associated with the differences in the resistance provided by cohesive soil when compared to the non-cohesive soil. As show in Fig. 1(a) and in Fig. 1(b), the cohesive soil considered in the analyses tend to have lower soil resistance when compared to the non-cohesive soil. Due to this, during dynamic analyses, the non-cohesive soil offers greater resistance to the loads at lower depths, pushing the point of fixity to 1D (-6.5m) and, consequently, experiencing the highest bending moment at this level. Meanwhile, for the cohesive, because of its lower soil resistance, the point of fixity remain at 2D (-12.5 m) or deeper 4D (-24.5 m).

5.2 Non-cohesive and cohesive soil comparison

Overall, the damage, in the critical region, experienced by the structures in cohesive soil were greater than for the non-cohesive soil. However, within cohesive soil, for lower undrained shear strength, the fatigue damage were greater, in any environmental state, as shown in Fig. 4(a). Same pattern was identified with structures in non-cohesive soil, which shows that lower internal angle of friction leads to greater damages, regardless of the environmental state, as shown in Fig. 4(b).

It shows how important it is to consider a coupled soil-structure analyses when it comes to fatigue estimation. Changes in the soil resistance leads to different natural frequencies, what in turn will increase or decrease the fatigue damage sustained by the structure, regardless of wave and wind action, in the respective critical region. For quantitative results, the Table 5 shows a summary of the normalized fatigue damage according to soil type. Following these results, a reduction of 28% in the internal friction angle led to a increase of 74% in the fatigue damage. While, for cohesive soil, a reduction of 80% in the undrained shear strength led to a increase of 739% in the fatigue damage.

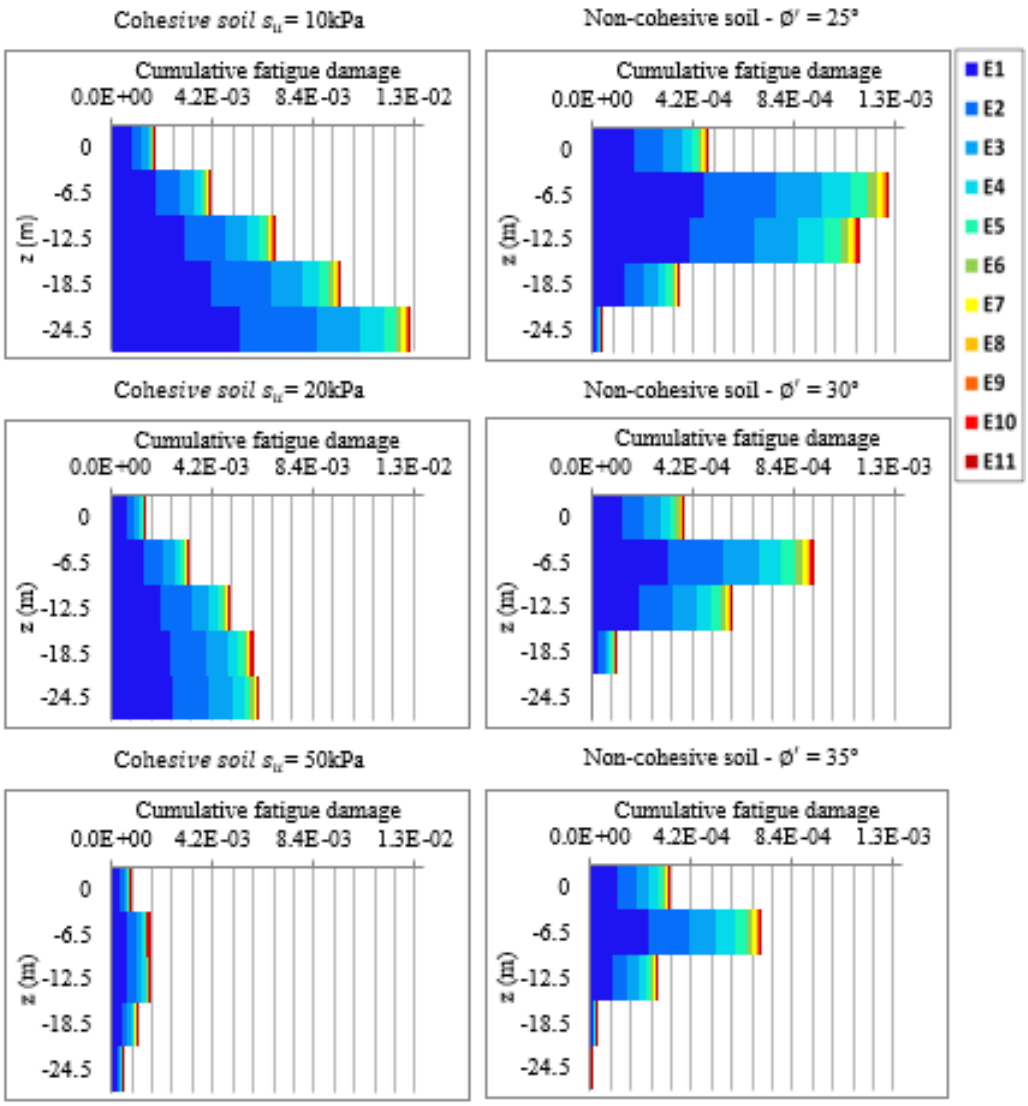

Figure 2. Cumulative fatigue damage according to region along the monopile.

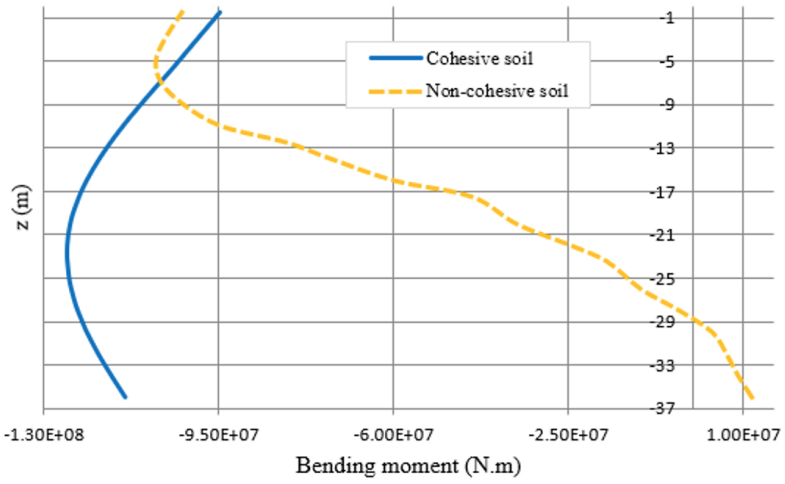

Figure 3. Maximum bending moment envelop

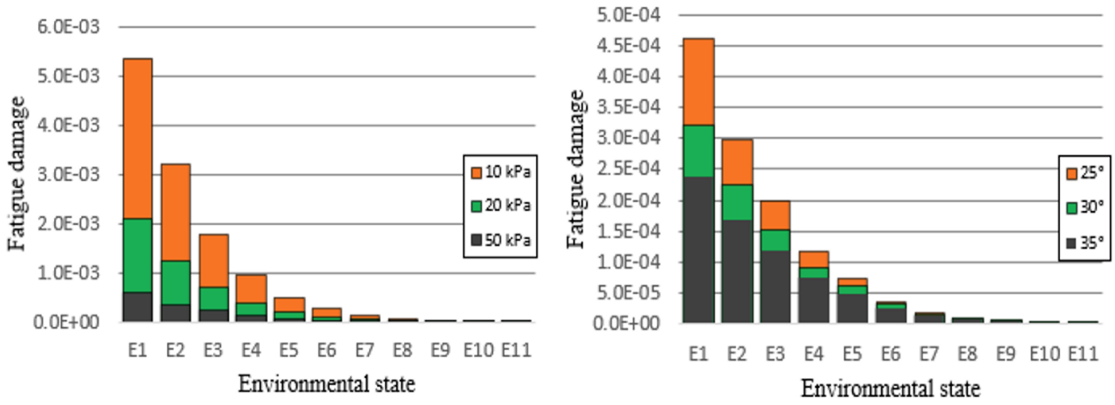

(a) Cohesive

(b) Non-cohesive

Figure 4. Fatigue damage contribution of the environmental state for cohesive and non-cohesive soil. Bars are overlaid.

Table 5. Normalized fatigue damage (NFD) according to soil type

Undrained shear strength	NFD	Internal friction angle	NFD
10 kPa	8.39	25°	1.74
20 kPa	3.31	30°	1.31
50 kPa	1	35°	1

6 Conclusions

The closing remarks for this study are:

- It was identified that, for the conditions adopted, the critical region was localized at 1D (-6.5 m) for cohesive soil and at 2D (-12.5 m) onwards for non-cohesive soil. This is due to a higher stiffness provided by the non-cohesive soil at lower depths as compared to the cohesive soil. This trend was both identified in the maximum bending moment envelop (Fig. 3) and in the cumulative fatigue damage along the monopile (Fig. 2);
- The lower the undrained shear strength (cohesive soil) and the internal angle of friction (non-cohesive soil), the greater will be the fatigue damage, regardless of the environmental state. As shown in Table 3, lower values of angle of friction and of undrained shear strength led to higher natural period, which indicates a more flexible structure. This higher flexibility leads to higher amplitude of vibration and, consequently, higher damages. This also explains why the cohesive soil sustained higher damages when compared to the non-cohesive soil, as the former allows the structure to vibrate more freely because of its less stiff soil;
- It was identified a increase of 74% in the damage for a reduction of 28% in the internal angle of friction for the non-cohesive soil. Whereas, for the cohesive soil, it was identified a increase of 739% in the fatigue damage for a reduction of 80% in the undrained shear strength.

Acknowledgements. The work presented in this paper is the result of a partnership between Petrobras and UFRJ and was carried out with funds from the R&D from program of the Eletric Sector regulated by ANEEL under the PD-00553-0045/2016 project, entitled ”Planta Piloto de Geração Eólica Offshore”.
The authors also thank the National Council for Scientific and Technological Development (CNPq) for the research grant PQ 308403/ 2016-9 and Petrobras for allowing the publication of this work. This study was also financed in part by the Coordenação de Aperfeiçoamento de Pessoal de Nível Superior-Brasil (CAPES), Finance Code 001, and by the Fundação Carlos Chagas de Amparo à Pesquisa do Estado do Rio de Janeiro (FAPERJ).

Authorship statement. The authors hereby confirm that they are the sole liable persons responsible for the authorship of this work, and that all material that has been herein included as part of the present paper is either the property (and authorship) of the authors, or has the permission of the owners to be included here.

References

[1] Lee, J. & Zhao, F., 2020. Global wind report 2019. Technical report, Global Wind Energy Council (GWEC), Brussels, Belgium.
[2] Gomes, F. A., 2019. Fatigue analysis of an offshore wind turbine of the monopile type with grouted connection. Master's thesis, Federal University of Rio de Janeiro, RJ, Brazil.
[3] Jonkman, J., Butterfield, S., Musial, W., & Scott, G., 2009. Definition of a 5-mw reference wind turbine for offshore system development. Technical report, National Renewable Energy Lab.(NREL), Golden, CO (United States).
[4] Marintek, 2013. Riflex theory manual v4.10.3.
[5] API-RP-2GEO, 2011. Geotechnical and foundation design considerations.
[6] DNVGL-ST-0126, 2016. Support structures for wind turbines. *Oslo, Norway: DNV*, vol. .
[7] Ruigrok, J. A. T., 2010. Laterally loaded piles, models and measurements. Master's thesis, Delft University of Technology, Netherlands.
[8] ISO-19902, 2007. Petroleum and natural gas industries–fixed steel offshore structures. *English version EN ISO*, vol. 19902, pp. 182–202.
[9] Gonçalves, R. T., Matsumoto, F. T., Malta, E. B., Medeiros, H. F., & Nishimoto, K., 2010. Conceptual design of monocolumn production and storage with dry tree capability. *Journal of offshore mechanics and arctic engineering*, vol. 132, n. 4.
[10] IEC-61400-3, 2009. Wind turbines—part 3: Design requirements for offshore wind turbines. *International Electrotechnical Commission and others*, vol. .
[11] Jonkman, B. & Kilcher, L., 2012. Turbsim user's guide: version 1.06. 00. *National Renewable Energy Laboratory: Golden, CO, USA*, vol. .
[12] Velarde, J. & Bachynski, E. E., 2017. Design and fatigue analysis of monopile foundations to support the dtu 10 mw offshore wind turbine. *Energy Procedia*, vol. 137, pp. 3–13.
[13] DNVGL-RP-C203, 2016. Fatigue design of offshore steel structures. *Oslo, Norway: DNV*, vol. .